Coupling between bulk thermal defects and surface segregation dynamics

Jonathan Li,[1,*] Siming Zhang [2,*] Chaoran Li,[1] Yaguang Zhu,[1] Jorge Anibal Boscoboinik,[3] Xiao Tong,[3]
Jerzy T. Sadowski [3] Guofeng Wang [2,†] and Guangwen Zhou [1,‡]

[1]*Department of Mechanical Engineering & Materials Science and Engineering Program,
State University of New York, Binghamton, New York 13902, USA*

[2]*Department of Mechanical Engineering and Materials Science, University of Pittsburgh, Pittsburgh, Pennsylvania 15261, USA*

[3]*Center for Functional Nanomaterials, Brookhaven National Laboratory, Upton, New York 11973, USA*

Surface segregation is a phenomenon that depends on the delicate interplay between thermodynamic driving forces and kinetic obstacles, for which elevated temperature is often needed to enhance the atom mobility and reach equilibrium. Using the classic system of $Cu_3Au(100)$ under nonisothermal conditions, herein, we show an adatom process underlying transient surface segregation dynamics through the temperature-change-driven creation and annihilation of thermal vacancies in the bulk and the resulting bulk-surface mass exchanges. This is demonstrated by monitoring the surface composition evolution of $Cu_3Au(100)$ with temperature changes between 250 and 500 °C, showing that the increase in temperature decreases monotonically the surface Au concentration as a result of the transfer of more Cu than Au from the bulk to the surface to form Cu-rich clusters of adatoms. Such a bulk thermal defect effect is expected to be universal in inducing the disparity in the bulk-surface mass exchanges of dissimilar atoms in multicomponent materials because of the inherent differences in the vacancy formation energies of the constituent atoms.

I. INTRODUCTION

Surface segregation phenomena in alloys cause the surface composition to differ from the bulk composition [1,2]. This process is of broad interest because it can be used to alter many material properties such as wetting, oxidation, corrosion, and catalysis [3–5]. Since most materials are alloys by design through the addition of alloying elements, by impurities after processing, or by contamination from the environment, surface segregation has been studied a great deal, and most of the work has been devoted to identifying the driving forces and predicting the existence of surface enrichment and the nature of the segregating components. Surface segregation is driven by an interplay between the thermodynamic driving forces and the kinetic process of atom mobility. The thermodynamic driving forces include difference in surface energies of the alloy components (the constituent metal with the lower surface energy tends to segregate to the surface), the relief of bulk lattice strain (larger atoms are favored on the surface because the surface can relax to accommodate them better than it is possible in the bulk), and the enthalpy of sublimation. Elevated temperature is typically required to overcome the kinetic obstacles and enhance the atom mobility in a segregation process.

Surface segregation is also influenced by chemical ordering tendencies that may hamper surface segregation [2,6–13]. This is because segregation favors the occupation of neighboring lattice sites by the same atomic species at the surface sites, whereas chemical ordering causes exactly the opposite. Therefore, there is a competition between surface segregation and chemical ordering. For an alloy with weak pairwise interactions of atoms, the alloy is a disordered solid solution, and the degree of surface segregation decreases as temperature increases [2]. For an alloy with strong pairwise interactions between atoms, the alloy is in an ordered state, and the degree of surface segregation increases, reaching a maximum, then decreases with the increase in temperature [14]. Usually, the competition between surface segregation and chemical ordering results in maximum segregation around the bulk order-disorder transition temperature of the alloy [2,14–16].

Most of the reported studies of segregation phenomena in extended surfaces of single crystals have been devoted to equilibrium segregation and are based on the assumed planar surfaces [2,13,14,17–19]. The planar surface configuration could be achieved for well-annealed crystals but may not be the case before the equilibrium segregation is established. This is shown in this paper by employing synchrotron x-ray photoelectron spectroscopy (XPS) to dynamically monitor the surface composition evolution of $Cu_3Au(100)$, where the high photon flux of the synchrotron x ray provides the sufficient temporal resolution to reveal transient segregation phenomena under nonisothermal conditions. In contrast to the common expectation of Au surface segregation driven by the lower surface energy of the constituent metals and the relief of bulk lattice strain (atom size effect) [13,16–27], we show that the surface concentration of Au monotonically decreases as the

*These authors contributed equally to this work.

†guw8@pitt.edu

‡gzhou@binghamton.edu

temperature increases from 250 to 550 °C, which corresponds to the surface enrichment of Cu at the higher temperature. Along with low-energy ion scattering (LEIS), scanning tunneling microscopy (STM) imaging, and atomistic modeling, these results show that this segregation behavior is induced by a close coupling between bulk thermal defects and surface segregation dynamics through the temperature-change-driven creation and annihilation of thermal vacancies in the bulk, which results in the formation of adatoms on the surface through the bulk-surface mass exchanges.

Thermal vacancies are a common type of structure defect in materials. As temperature increases, the concentration of thermal vacancies increases and affects various properties of materials, such as melting point, heat capacity, diffusivity, and thermal conductivity [28–31]. Although surfaces are known as sinks or sources of thermal vacancies, the effect from the creation and annihilation of bulk thermal vacancies has not been considered in studying segregation phenomena. In this paper, we show that the temperature-dependent concentration of bulk thermal vacancies results in the exchange of the bulk thermal vacancies with the surface, which makes an apparent contribution to the evolution of the surface composition and morphology of multicomponent materials. The identified bulk-surface coupling phenomenon may find broader applicability in other alloy systems. This is because the inherent disparity in the equilibrium concentrations of thermal vacancies of the constituent atoms in multicomponent materials can result in the disparity in the transfers of the constituent atoms between the surface (or internal interfaces) and bulk with temperature changes. The coupling between bulk thermal defects and surface segregation dynamics may manifest itself in influencing many surface properties that are sensitive to variations in surface compositions.

II. EXPERIMENTAL AND COMPUTATIONAL METHODS

Ambient pressure (AP) XPS was employed to monitor the surface composition evolution of $Cu_3Au(100)$ as a function of temperature. The AP-XPS experiments were performed at the IOS beamline of the National Synchrotron Light Source II (NSLS-II), Brookhaven National Laboratory. The AP-XPS endstation is equipped with a main chamber with the base pressure $< 5 \times 10^{-9}$ Torr, a SPECS Phoibos NAP 150 hemispherical analyzer, and an Ar-ion sputtering gun. The multiple differential pumping stages between the main chamber and the hemispherical analyzer allow us to maintain ultrahigh vacuum (UHV) conditions ($< 1 \times 10^{-7}$ Torr) in the analyzer when the pressure in the main chamber is a few Torr. Photoemitted electrons leave the high-pressure chamber through a small aperture in a conical piece into the differentially pumped transfer lenses system toward the electron energy analyzer, allowing for continuously acquiring XPS spectra at pressures of up to ∼5 Torr. The photon energy range of the beamline is from 250 to 2000 eV, which covers the O 1*s*, C 1*s*, Cu 2*p*, and Au 4*f* core levels relevant for this paper. Real-time monitoring of the surface composition evolution induced by surface segregation was performed by acquiring spectra of the Au 4*f* core level *in situ*.

The Cu_3Au single crystal (Princeton Scientific Corp, purity = 99.9999%) was a top-hat-shaped disc, cut to within 0.1° to

the (100) crystallographic orientation and polished to a mirror finish. The sample was heated via a ceramic button heater, and its temperature was measured by a type-K thermocouple. The crystal was cleaned by repeated cycles of Ar^+ bombardment (5×10^{-5} Torr of Ar gas, $1\,\mu A\,cm^{-2}$, 1.0 keV, 20 min) at room temperature followed by annealing at 550 °C (UHV, 10 min) until no O and C spectra could be detected by XPS at elevated temperature. All spectra were collected at a takeoff angle of 20° between the sample surface and the electron analyzer optics of the XPS spectrometer. Identification of the surface sensitivity of each species in the near-surface region was performed using depth profiling of the chemical composition by varying the incident photon energy from 400 to 1250 eV. Binding energies in each spectrum were referred to the Fermi level for correction and analyzed with the Voigt lineshape [32] and Shirley-type background [33]. Integrated peak areas of each Au species were used to calculate the relative composition evolution. Separate UHV systems equipped with low-energy electron diffraction (LEED), STM, and LEIS with a SPECS Phoibos 100 energy analyzer were used to further confirm the crystal structure and surface composition of the $Cu_3Au(100)$ prepared using a similar procedure to that in the AP-XPS measurements.

The density functional theory (DFT) calculations were carried out using the Vienna *ab initio* Simulation Package (VASP) [34]. Plane-wave basis associated with the projector augmented wave approach [35] was employed. The generalized gradient approximation with the Perdew-Burke-Ernzerhof (PBE) [36] exchange-correlation functional was used to evaluate the exchange-correlation energy. The plane-wave energy cutoff energy was set as 500 eV. In all calculations, the total energy of system was converged within 10^{-6} eV. In this paper, we modeled the $Cu_3Au(100)$ surface using a 20-layer slab cell, which has four atoms in each layer and contains a vacuum region of 12 Å in the direction normal to the surface. A Monkhorst-Pack [37] k-point grid of $6 \times 6 \times 1$ was used for these surface calculations. We also computed the energies of point defects in Cu_3Au $L1_2$ crystal, which was modeled using a $3 \times 3 \times 3$ superlattice containing 108 atoms. A Monkhorst-Pack k-point grid of $4 \times 4 \times 4$ was used for these bulk crystal calculations. All the structures were fully relaxed until the force acting on each atom was < 0.01 eV/Å. During the structural optimization of the surfaces, we fixed the atoms in the bottom five layers at their bulk crystal determined positions and allowed all the other atoms fully relax.

III. RESULTS

A. Experimental measurements

The structure of the ordered and disordered Cu_3Au and the associated order-disorder phase transition have been studied in detail in the bulk and at the surface [13,16,24,25]. The $L1_2$-ordered $Cu_3Au(100)$ surface could be terminated in a plane of pure Cu (i.e., CuCu plane) or in a plane consisting of equal numbers of Cu and Au atoms (CuAu plane). Surface science experiments have shown that the $Cu_3Au(100)$ surface is terminated with the CuAu plane [17–19]. As shown in Fig. 1(a), the parameters of the two cells marked in Fig. 1(a) are related by $b = \sqrt{2}a$ with the 45° rotation angle of the
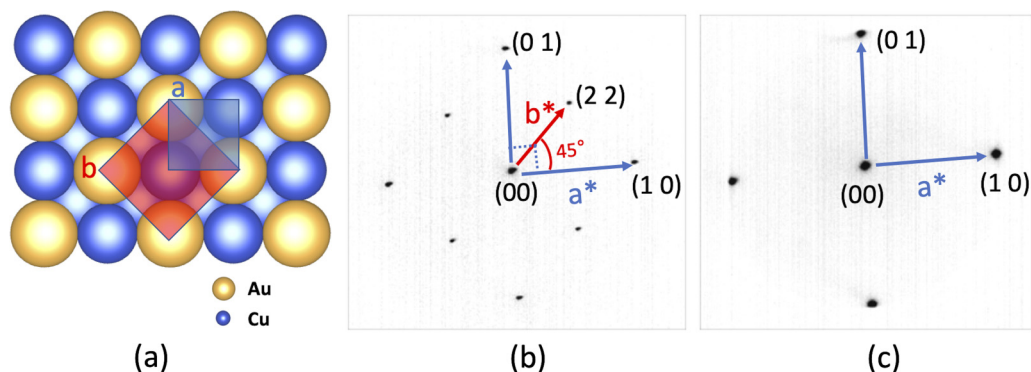
FIG. 1. (a) Wood's notation of the $c(2 \times 2)$ surface structure of ordered $Cu_3Au(100)$. (b) Low-energy electron diffraction (LEED) pattern obtained from $Cu_3Au(100)$ at 250 °C, where the spot (2,2) corresponds to the superlattice cell (b) shown in (a). (c) LEED pattern obtained at 500 °C, in which the superlattice spot (2,2) disappears, indicating that the surface becomes chemically disordered. Primary electron energy: $E_p = 25$ eV.

two cells; this makes the Wood's notation of the surface structure of the $(\sqrt{2} \times \sqrt{2})R45°$ or $c(2 \times 2)$ (i.e., cell a). Figure 1(b) is a LEED pattern obtained from the clean surface of the $Cu_3Au(100)$ crystal that was well annealed at ~ 250 °C, which shows sharp diffraction spots of the $c(2 \times 2)$ superstructure, indicating that the surface practically preserves the chemical ordering of the bulk termination of the CuAu plane. Figure 1(c) is a LEED pattern obtained from the $Cu_3Au(100)$ at ~ 500 °C, showing that the spots associated with the superlattice structure (i.e., cell b) disappear. This confirms that the surface becomes chemically disordered at the elevated temperature, consistent with the previous studies showing that the surface long-range order parameter is unity at temperatures $<\sim 230$ °C but drops to zero at the bulk order-disorder transition temperature of 390 °C [22,38–40].

We therefore used AP-XPS to monitor the surface composition evolution of the $Cu_3Au(100)$ for both the ordered and disordered phases by varying the crystal temperature between 250 and 500 °C. To ensure that an intrinsic segregation behavior was studied, the XPS measurements were comparatively performed under both UHV conditions and in H_2 gas flow of ~ 1 Torr, where the latter provided a reducing gas environment to further maintain the surface cleanliness by preventing any residual oxygen contamination. The comparative XPS measurements indicate that there was no noticeable difference in the surface segregation behavior between the UHV conditions and H_2 gas flow, confirming the cleanliness and pristine nature of the crystal surface under both UHV and in the H_2 gas flow. The lack of reactivity of the pristine $Cu_3Au(100)$ toward H_2 molecules can be attributed to the high dissociation barriers of H_2 molecules on metallic Cu and Au surfaces [41–43]. Even for atomic H, it bonds weakly to Cu and Au and desorbs readily from Au surfaces above -163 °C [44] and from Cu surfaces $>\sim 22$ °C [45].

Figure 2(a) shows XPS spectra of the Au $4f$ peaks obtained from the $Cu_3Au(100)$ at 250 °C with the incident photon energies of 400 and 1250 eV, respectively. The Au $4f$ region contains two contributions corresponding to Au $4f_{7/2}$ and Au $4f_{5/2}$, respectively. Both contributions can be deconvoluted into two components, labeled S and B and located at the binding energies (BEs) of 84.5 and 84.0 eV for Au $4f_{7/2}$ and 88.2 and 87.7 eV for Au $4f_{5/2}$, respectively. The two

components correspond to surface (S) Au and bulk (B) Au, and their binding energies are consistent with previous reports on Cu-Au alloys [46–52]. The relative position of the B and S components is further distinguished with depth profiling by varying the photon energies of the incident x ray. As shown in Fig. 2(a), the peak associated with the S component appears stronger with the lower photon energy of 400 eV. This indicates that the S component is indeed more surface sensitive than the B component. Figure 2(b) shows typical XPS spectra of the corresponding Cu $2p$ region, where the absence of shakeup satellites between the Cu $2p_{1/2}$ peak and the Cu $2p_{3/2}$ peak indicates that Cu is in the metallic state. The surface cleanliness was further confirmed by the absence of any detectable intensity from the O $1s$ region, as also shown in Fig. 2(b).

We then examined the surface composition evolution of the $Cu_3Au(100)$ crystal with increasing temperature in UHV. Figure 3(a) shows the XPS spectra of the Au $4f$ peaks by annealing the Cu_3Au crystal from 250 to 500 °C. The crystal was held at each temperature for about 10 min for possible equilibration and reaching a steady composition. Once no noticeable changes in the XPS peak intensities were detected, the temperature was increased. Surprisingly, we observed that
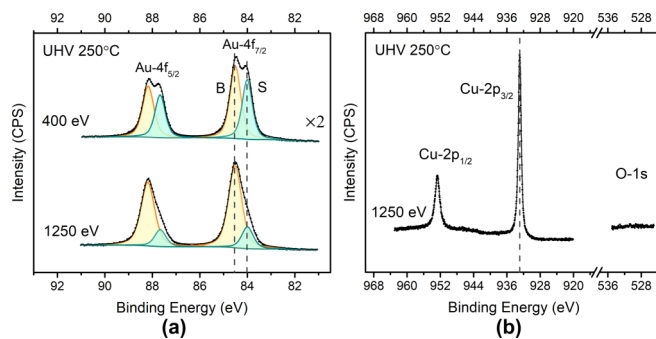

FIG. 2. (a) Photoelectron spectra of the Au $4f$ region of $Cu_3Au(100)$ under ultrahigh vacuum (UHV) annealing at 250 °C. S, in light green, corresponds to the surface Au contribution, while B, in yellow, corresponds to the bulk Au contribution. (b) Photoemission spectra of the Cu $2p$ and O $1s$ regions of the $Cu_3Au(100)$ under UHV and at 250 °C.
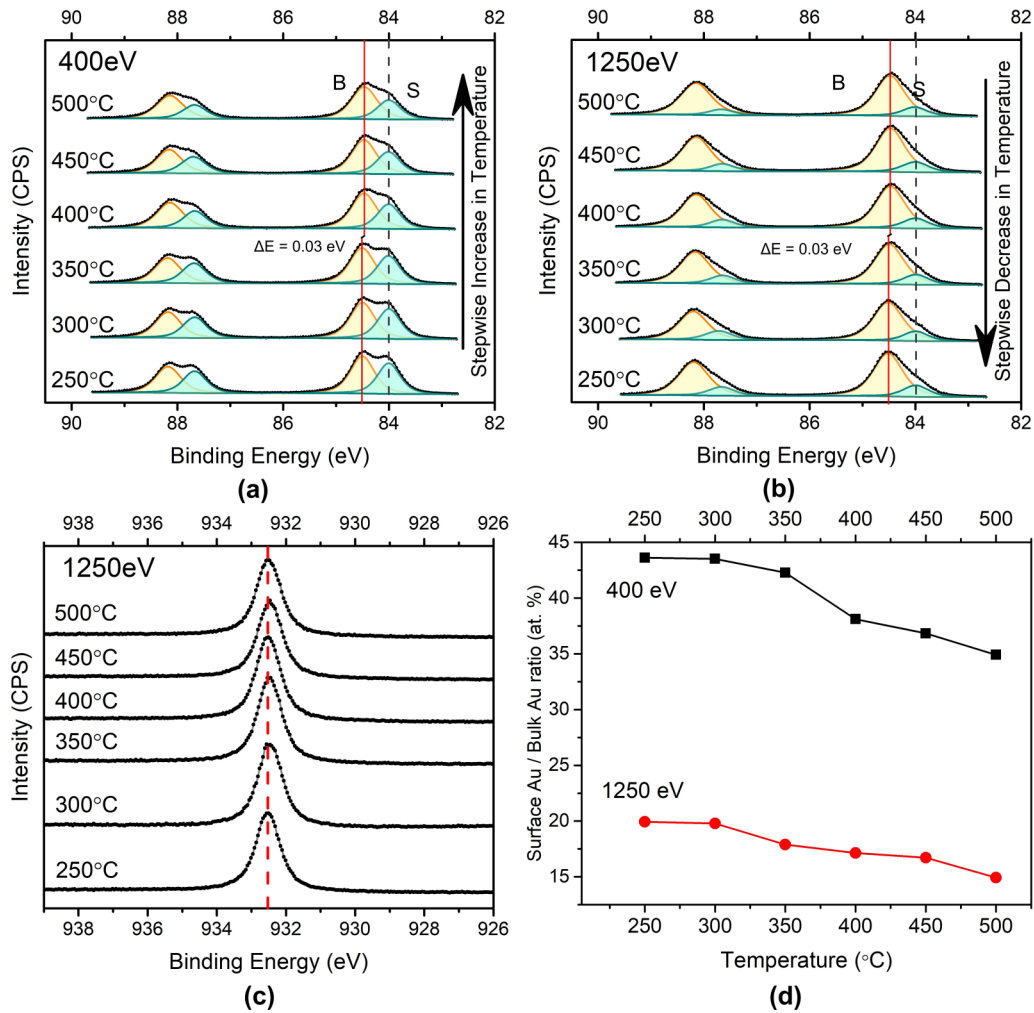
FIG. 3. (a) Au $4f$ x-ray photoelectron spectroscopy (XPS) spectra of the $Cu_3Au(100)$ measured at the incident photon energy of 400 eV as the temperature increases from 250 to 500 °C. A stepwise increase in temperature is applied after a saturated peak intensity is established at each temperature. (b) and (c) Au $4f$ and Cu $2p$ spectra of the $Cu_3Au(100)$ taken at the photon energy of 1250 eV upon the stepwise decrease in temperature from 500 to 250 °C. (d) Evolution of the percentage of the surface Au component by quantifying the Au $4f$ XPS spectra of the $Cu_3Au(100)$ measured with the photon energies of 400 and 1250 eV upon the stepwise variation in temperature between 250 to 500 °C. The measurements with both photon energies confirm that the surface Au component decreases as the temperature increases.

the surface Au peak S decreases monotonically in intensity as the temperature increases, whereas the bulk Au component B remains relatively constant, suggesting that the surface Au concentration decreases as the temperature increases. This appears counterintuitive because the higher temperature promotes atom mobility, and thus, more Au segregation to the surface should be expected (Au has a lower surface energy and larger atom size than Cu, both of which favor Au segregation to the surface to reduce the surface energy and release bulk lattice strain). To further confirm the temperature-dependent evolution of the surface Au and bulk Au peaks shown in Fig. 3(a), XPS measurements were also performed to check the reversibility of the evolution of peak intensities by lowering the crystal temperature from 500 to 250 °C. A higher incident photon energy of 1250 eV was used for the measurements, which not only allowed for monitoring the intensity evolution of the two Au species but also for further examining their relative locations at each temperature by comparing the peak intensity obtained with the lower photon energy

in Fig. 3(a). As shown in Fig. 3(b), the surface Au peak increased in intensity as temperature decreased, whereas the bulk Au peak remained relatively constant, confirming the reversibility of the evolution of the two Au components upon the temperature swing between 250 and 500 °C. It can be also noted from Fig. 3(b) that the intensity of the surface Au peak is relatively weaker than that shown in Fig. 3(a), further confirming the surface nature of the surface Au component at each temperature.

It is worth mentioning that composition changes in the Cu-Au system do not induce apparent chemical shifts in XPS. This was demonstrated by Kuhn and Sham [53] in a detailed XPS study of a series of Au-Cu alloys of various stoichiometries and order, showing that the Au $4f$ chemical shift is merely 0.06 eV among pure Au, AuCu, and $AuCu_3$. Our XPS results are consistent with this trend and show only an extremely small binding energy shift (0.03 eV) between 350 and 400 °C, which corresponds to the order-disorder transition in Cu_3Au. Therefore, the larger separation of the binding

energies between the surface and bulk components of Au is attributed to the geometric effect rather than the local chemical environment. One can also note from Figs. 3(a) and 3(b) that the peak intensity for the bulk component of Au remains relatively constant, while the surface Au peak decreases as the temperature increases. The decreased surface Au peak intensity can be induced by the expelling of more Cu than Au from the bulk to the surface at the higher temperature. The relatively constant peak intensity for the bulk component of Au can be attributed to the rapid compositional homogenization in the bulk (and the subsurface region probed by the XPS). This is due to the elevated temperatures examined here (250 to 550 °C) and the relatively small energy barriers for the diffusion of Au and Cu atoms in the bulk, as shown later in our DFT calculations.

Figure 3(c) shows the Cu $2p_{3/2}$ spectra taken with the photon energy of 1250 eV upon decreasing the temperature from 500 to 250 °C. The Cu $2p$ maintains the same binding energy of 932.5 eV at the different temperatures. This is consistent with previous XPS studies showing that the binding energy for Cu $2p$ is not sensitive to composition changes in Cu-rich alloys [53–55]. It is worth mentioning that all the spectra in Figs. 3(a)–3(c) are normalized to the background and thus show the absolute intensities of the spectra at the different temperatures. Figures 3(a)–3(c) also show that the total spectral intensities of Au $4f$ and Cu $2p$ decrease slightly as the temperature is increased from 250 to 550 °C. This is due to the heating effect, where the thermal expansion can induce dimensional changes to the sample stage and thus results in slight changes in the alignment between the sample and the XPS analyzer. This is also confirmed by the recovered XPS spectral intensities upon cooling the sample from 550 to 250 °C [i.e., Figs. 3(a) and 3(b)]. Such heating-induced changes to the global spectral intensities do not affect the quantification of the Au spectra [Fig. 3(d)], which is based on the ratio of the S and B peak areas of the XPS spectra obtained at the different temperatures.

The evolution of the integrated peak area of the surface Au and bulk Au components, shown in Figs. 3(a) and 3(b), can be quantified to determine the relative changes of the two Au species as a function of temperature increasing from 250 to 500 °C. Figure 3(d) illustrates the surface and bulk Au contents measured at the different temperatures with the photon energies of 400 and 1250 eV, respectively, both of which show a similar trend in the evolution of the two Au species. That is, the percentage of surface Au decreases monotonically as the temperature increases, irrespective of the crystal in the ordered or disordered phases. At 250 °C, the percentage of the surface Au composition is 43.5%, while the bulk Au composition is 56.5% measured with the photon energy of 400 eV. The surface Au contribution gradually decreases, while the alloy Au contribution increases with the increase in temperature. At 500 °C, the surface Au contribution is 34.9%, while the bulk Au contribution is 65.1%. The surface-Au-to-bulk-Au ratio decreases from 0.77 at 250 °C to 0.54 at 500 °C. For the measurements with the larger photon energy of 1250 eV, the percentage of the surface Au component is less because the larger sampling depth results in more contribution from the bulk Au.

To complement the above XPS measurements that provide information on the surface composition averaged over a few

atomic layers (i.e., over the thickness comparable with the mean free path of photoelectrons), LEIS was performed to monitor the temperature-dependent composition evolution in the topmost atomic layer only. The LEIS spectra were taken with 1.5 keV He$^+$ and the scattering angle of 135°, which ensured a good mass separation between Au and Cu in combination with a high detector efficiency. Figure 4(a) shows the LEIS spectra of Cu and Au measured with the stepwise increase in temperature. The crystal was held at each temperature for about 10 min to ensure the possible equilibration of the surface composition. Although LEIS is incapable of distinguishing between surface Au and bulk Au, it complemented the XPS measurements by providing composition information about the amount of Au and Cu in the topmost layer. Figure 4(b) illustrates the surface composition evolution by quantifying the integrated peak area of Cu and Au in the LEIS spectra in Fig. 4(a), showing that the Au concentration decreases, whereas the Cu concentration increases as the temperature increases. This indicates a decreased net amount of Au and an increased Cu amount in the topmost surface as the temperature increased, consistent with the trend derived from the XPS measurements.

B. Atomistic modeling

1. DFT modeling of the surface segregation in $Cu_3Au(100)$

To further differentiate the microscopic pathways and gain insights into the mechanism of the experimentally observed segregation phenomenon, we also performed DFT calculations to predict the surface segregation of the ordered $Cu_3Au(100)$ surface and diffusion energetics associated with the surface segregation dynamics. In the unit cell of Cu_3Au $L1_2$ bulk crystal, one Au atom occupies the corner, and three Cu atoms lie at the face centers of a face-centered cubic (fcc) lattice. Our DFT calculation predicts its equilibrium lattice parameter to be 3.79 Å, which is in good agreement with experiment value of 3.75 Å [56] and the theoretical calculation result of 3.78 Å [57]. From the equilibrium Cu_3Au $L1_2$ bulk crystal, we constructed the Cu_3Au $L1_2$ (100) surface with two possible terminations. The outermost surface layer contains 50% Au and 50% Cu in one case [denoted as $(100)_A$] and 100% Cu in the other case [denoted as $(100)_B$].

We first examined the possibility of the equilibrium segregation of the planar (100) surface. Following the direct exchange mechanism as illustrated in Fig. 5, we used the DFT method to calculate the Au *surface segregation energy*, which is defined as the energy difference for exchanging the positions of the subsurface Au atoms with the Cu atoms in the outermost layer of the $Cu_3Au(100)$ surface. A negative value of the Au surface segregation energy indicates a preference of Au to segregate to the outermost layer from the subsurface. For the Cu_3Au $L1_2$ $(100)_A$ surface, we calculated the energies of three Au surface segregated models. As compared with the bulk-terminated surface [Fig. 5(a)], we exchanged $\frac{1}{4}$ layer of Au atoms in the third subsurface layer with $\frac{1}{4}$ layer of Cu atoms in the outermost layer in Fig. 5(b), exchanged $\frac{1}{2}$ layer of Au atoms in the third subsurface layer with $\frac{1}{2}$ layer of Cu atoms in the outermost layer in Fig. 5(c), and exchanged $\frac{1}{4}$ layer of Au atoms in the third subsurface layer as well
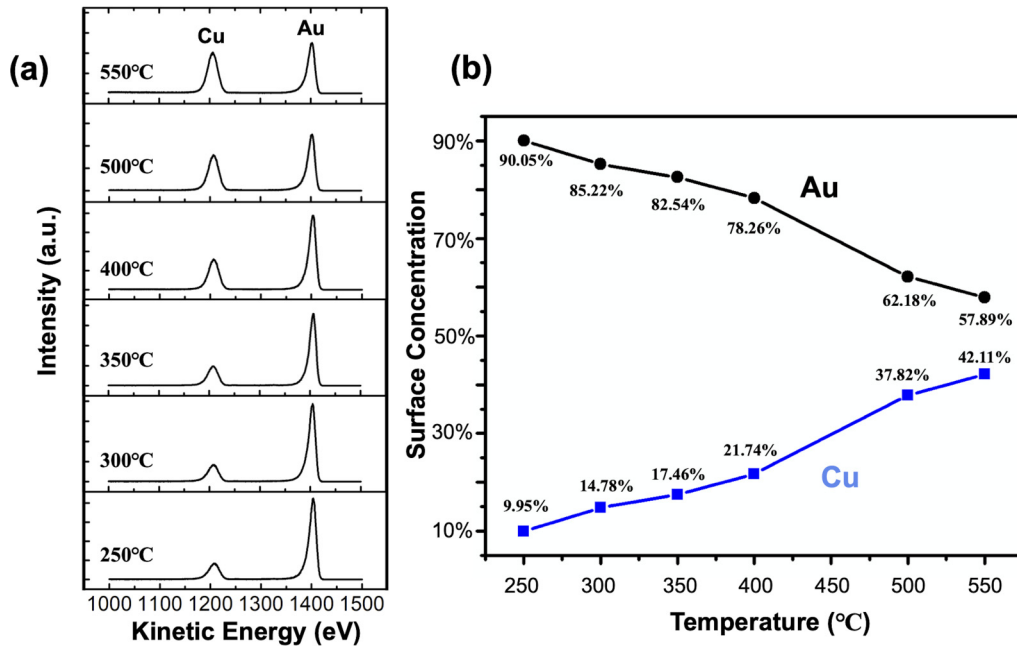
FIG. 4. (a) Low-energy ion scattering (LEIS) spectra of Au and Cu obtained from the $Cu_3Au(100)$ upon the stepwise increase in temperature from 250 to 500 °C. A saturated peak intensity is reached at each temperature. (b) Evolution of the Cu and Au composition as a function of temperature.

as $\frac{1}{4}$ layer of Au atoms in the fifth subsurface layer with $\frac{1}{2}$ layer of Cu atoms at the outermost layer in Fig. 5(d). Our DFT results in Table I clearly indicate that it is energetically unfavorable for Au surface segregation to occur through these three direct-exchange routes.

For the Cu_3Au $L1_2$ $(100)_B$ surface, we calculated the energies of three Au surface segregated models. As compared with the bulk-terminated surface [Fig. 5(e)], we exchanged $\frac{1}{4}$ layer of Au atoms in the second subsurface layer with $\frac{1}{4}$ layer of Cu atoms in the outermost layer in Fig. 5(f), exchanged $\frac{1}{2}$ layer of Au atoms in the second subsurface layer with $\frac{1}{2}$ layer of Cu atoms in the outermost layer in Fig. 5(g), and exchanged $\frac{1}{2}$ layer of Au atoms in the second subsurface layer as well as $\frac{1}{2}$ layer of Au atoms in the fourth subsurface layer with a whole Cu outermost layer in Fig. 5(h). Although our DFT results in Table I indicate that it is indeed energetically
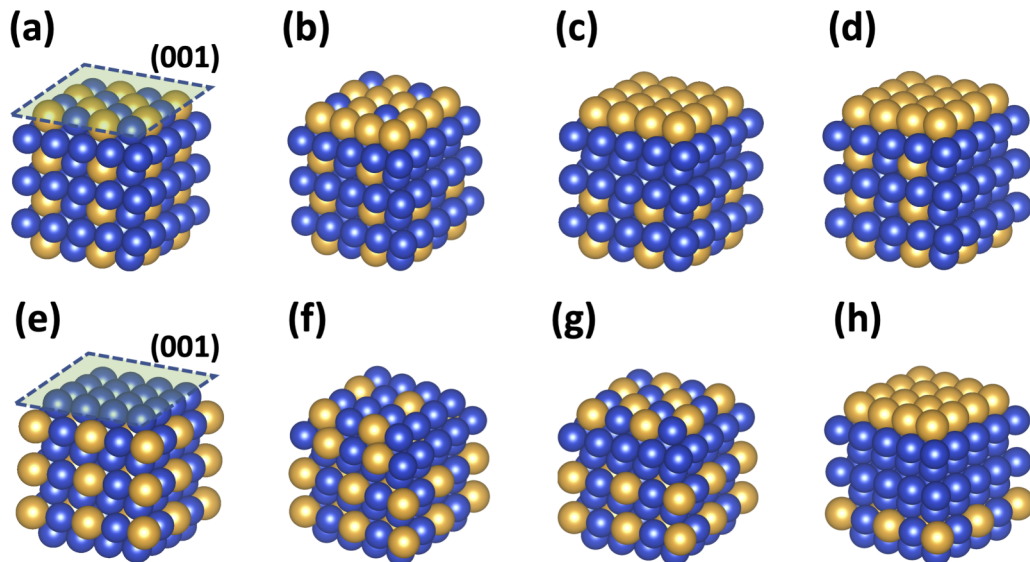

FIG. 5. Atomic structures of Cu_3Au $L1_2$ (100) surfaces. (a) Bulk-terminated $(100)_A$ with an outermost layer containing 50% Au, (b) Au surface-segregated $(100)_A$ with an outermost layer containing 75% Au, (c) and (d) Au surface-segregated $(100)_A$ with an outermost layer containing 100% Au, (e) bulk-terminated $(100)_B$ with an outermost layer containing no Au, (f) Au surface-segregated $(100)_B$ with an outermost layer containing 25% Au, (g) Au surface-segregated $(100)_B$ with an outermost layer containing 50% Au, and (h) Au surface-segregated $(100)_B$ with an outermost layer containing 100% Au. The blue and yellow balls represent Cu and Au atoms, respectively.

TABLE I. Predicted Au surface segregation energy (in units of electronvolts) of the Cu_3Au $L1_2$ (100) surfaces. The corresponding structures are presented in Fig. 5. Positive (or negative) values indicate resistance (or preference) of Au surface segregation.

$(100)_A$		$(100)_B$	
(a) → (b)	0.171	(e) → (f)	−0.367
(a) → (c)	0.269	(e) → (g)	−0.876
(a) → (d)	0.332	(e) → (h)	−0.635

favorable for Au surface segregation to occur through these three direct-exchange routes, we predict that the surface structure, which has a 50% Au and 50% Cu in the outermost layer and 100% Cu in the second layer, would have the lowest energy. Actually, this surface structure [Fig. 5(g)] has the same top two layers as the bulk-terminated Cu_3Au $L1_2$ $(100)_A$ surface. To demonstrate the stability of this surface termination (i.e., 50% Au and 50% Cu) against any other possible surface segregation configurations, we further predicted the energy changes for exchanging a single Au atom in the third, fifth, or seventh subsurface layer with one Cu atom in the outermost layer, as well for exchanging a single Cu atom in the second, third, or fifth subsurface layer with one Au atom in the outermost layer. Our DFT results indicate that all these surface structure modifications lead to the increased system energies and hence are thermodynamically unfavorable.

2. Temperature dependence of Au surface segregation

The above calculation results demonstrate that the bulk terminated Cu_3Au $L1_2$ (100) (i.e., 50% Au and 50% Cu) is the most stable segregation configuration for the planar surface. Such equilibrium segregation of the planar surface cannot explain the experimental observations, showing that the surface composition evolves from $\sim 90\%$ Au at 250 °C to 50% Au at 550 °C. Therefore, we further modeled the kinetic aspects of the segregation including the formation of Cu and Au vacancies in the bulk, vacancy-assisted diffusion of Cu and Au atoms in the bulk, and the formation of Cu and Au adatoms by out-of-surface diffusion. First, we performed DFT calculations to predict the formation energies of point defects and the migration energies for vacancy-assisted diffusion in $L1_2$ Cu_3Au crystal. Here, the point defects include specifically Cu vacancy (V_{Cu}) and Au vacancy (V_{Au}). The vacancy formation energies of these point defects were calculated as $E_f = E_v - E_0 + \mu$, where E_v is the energy of the crystal containing a vacancy, E_0 is the energy of the perfect crystal, and μ is the chemical potential of an Au or Cu atom. In this paper, the chemical potential of an Au or Cu atom is assumed to be the energy per atom in fcc Au or fcc Cu crystal. Thus, we predict that the formation energies are 0.75 eV for a Cu vacancy and 1.53 eV for an Au vacancy, respectively. These DFT results suggest that there would be more Cu vacancies with the lower formation energy than Au vacancies with the high formation energy in typical $L1_2$ Cu_3Au crystal samples. It has been reported that the employed PBE functional leads to pronounced underestimation of the cohesive energy in fcc Au crystal [58]. A correction to this known issue will lead to even higher formation energy of Au vacancy than that

of Cu vacancy in Cu_3Au crystal and would not change our conclusion of this paper.

Furthermore, we calculated the migration energies for vacancy-assisted diffusion of Cu and Au atoms in $L1_2$ Cu_3Au crystal using the nudged elastic band (NEB) method [59]. In each NEB calculation, we used three intermediate images to locate the transition state and calculated the migration energy as the energy difference between the transition state and the initial state. In $L1_2$ ordered Cu_3Au crystal, each Cu atom is nearest neighbored by eight Cu atoms and four Au atoms, whereas each Au atom is nearest neighbored by 12 Cu atoms. Therefore, in an elementary step of the vacancy-assisted diffusion, a Cu atom could move into an adjacent Cu vacancy or an Au vacancy. In contrast, an Au atom could only move into an adjacent Cu vacancy. Here, we predict that the migration energy for a Cu atom diffusing to an adjacent Cu vacancy is 0.65 eV ($\sim$0.63 eV from Ref. [57]), the migration energy for a Cu atom diffusing to an adjacent Au vacancy is 0.43 eV (same as 0.43 eV from Ref. [57]), and the migration energy for an Au atom diffusing to an adjacent Cu vacancy is 1.01 eV ($\sim$1.02 eV from Ref. [57]). These results indicate that it requires a lower migration energy barrier for Cu atoms to diffuse through the crystal than the Au atoms. Hence, Cu is the faster migrating species in the Cu_3Au crystal. Therefore, our DFT calculations provide a mechanistic understanding of the experimental results that the Au concentration in the Cu_3Au (100) surface would decrease with increasing temperature. Our computational results suggest that increasing temperature leads to generation of more thermal vacancies in the bulk, and the Cu atoms diffuse outward faster than the Au atoms through the crystal. Consequently, the surface will have an increasing concentration of Cu at elevated temperature.

In addition, we computationally examined the energy barriers for the surface-bulk mass exchanges that require the diffusion of atoms out of the planar surface. To this end, we first evaluated the formation energy of Au and Cu adatoms on the surface. This was modeled by displacing one Au (or Cu) atom to its nearest hollow or bridge sites of the Cu_3Au $L1_2$ $(100)_A$ surface (as shown in Fig. 6) to form an Au (and Cu) adatom. The formation energy of the Au (or Cu) adatom was obtained as the energy difference between the models with and without the surface adatom. Our DFT results show that the formation energies are 1.20 eV for both Au and Cu adatoms on the hollow site. In comparison, the formation energies of the adatoms at the bridge site are 1.59 eV for Au and 1.72 eV for Cu, respectively. These results indicate that the Au and Cu adatoms prefer to occupy the hollow site.

We then calculated the migration energies for the out-of-surface diffusion of Cu and Au atoms using the NEB method. In the initial state, the migrating Au and Cu atoms are at the lattice site of the planar surface. In the final state, the Au (or Cu) atom migrates to the nearest hollow site on the surface (because the hollow site is more favorable to host the adatom than the bridge site). Our NEB calculations show that the out-of-surface diffusion requires overcoming the energy barriers of 1.67 and 1.71 eV for the formation of Au and Cu adatoms, respectively. These out-of-surface migration energy barriers are much higher than the barriers for vacancy-assisted diffusion in the bulk, i.e., 0.65 (0.43) eV for Cu atom diffusing to an adjacent Cu (Au) vacancy site and 1.01 eV for Au atom
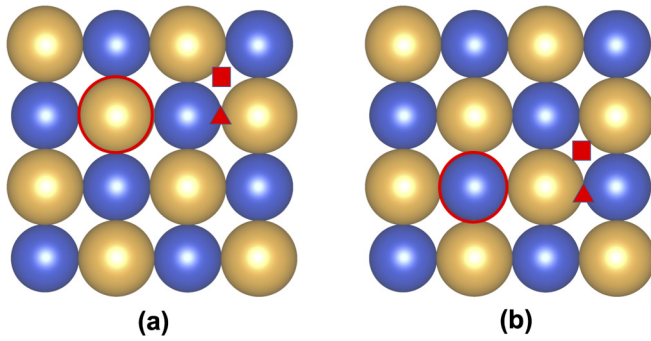
FIG. 6. Cu_3Au L1$_2$ (100)$_A$ surface consisting of two crystallographically nonequivalent surface sites for the formation of Au and Cu adatoms, that is, the hollow and bridge sites as indicated by the red square and triangle, respectively. (a) The formation of Au adatom by displacing a lattice Au atom (marked by the red circle) to its adjacent hollow or bridge site. (b) The formation of Cu adatom by the migration of a lattice Cu atom (marked by the red circle) to its adjacent hollow or bridge site. The blue and yellow balls represent Cu and Au atoms, respectively.

FIG. 7. Equilibrium concentrations of Cu and Au bulk vacancies in Cu_3Au at different temperatures.

diffusing to an adjacent Cu vacancy site. Consequently, the out-of-surface diffusion can be the rate-limiting step for the surface-bulk mass exchanges.

IV. DISCUSSION

The Cu-Au system has been extensively studied as a model system for understanding surface segregation phenomena. Previous studies mainly focused on determining the equilibrium segregation profile of the Cu-Au alloys using surface science tools such as Auger electron spectroscopy [26,27], LEIS [20–22], medium-energy ion scattering [23], and x-ray crystal truncation rod diffraction [16,24,25]. The temperature-dependent surface segregation depth profile of the Cu_3Au(100) was also measured, showing that the first layer of Cu_3Au(100) decreased from 50% in Au concentration at room temperature to 32% at 447 °C, where the decrease in the Au concentration was shown to be continuous rather than abrupt at the critical temperature of the order-disorder transition [23]. Above the order-disorder transition temperatures, the oscillatory decay of the Au composition was observed from the topmost surface down to several atomic layers of the subsurface region [16]. These previous studies dealt with well-annealed crystals, for which a planar surface with the Cu_3Au L1$_2$ (100) bulk termination consisting of equal numbers of Cu and Au atoms (CuAu plane, 50 at. % Au-50 at. % Cu) could be achieved [13,16–27]. Such a well-annealed crystal produces the equilibrium segregation profile. In contrast, here, we deal with the transient segregation behavior under the nonisothermal conditions, where the temperature-change-driven creation-annihilation of thermal vacancies in the bulk results in the mass transfer between the surface and bulk. Using the XPS measurements, as shown here, we monitor the surface composition evolution induced by the dynamic interplay between surface Au and bulk Au. These measurements demonstrate that the concentration of surface Au decreases with the increase in temperature, irrespective of the order or disorder phases of the crystal. The XPS results are also
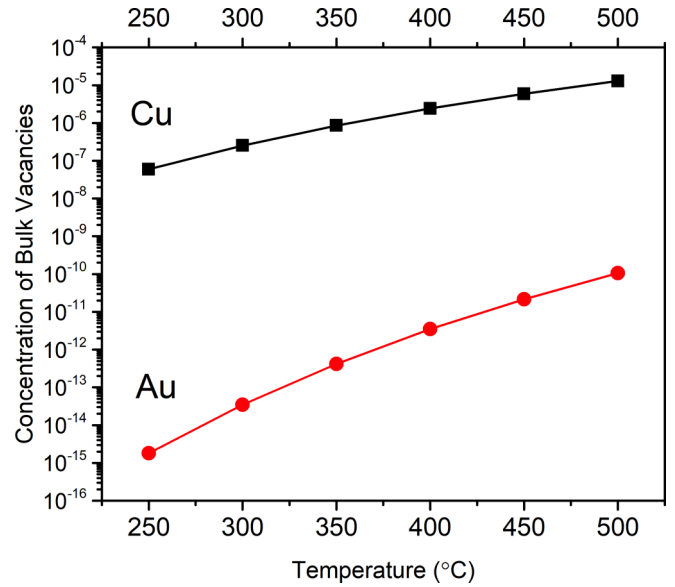
cross-validated by LEIS measurements, showing the Au surface composition evolution from nearly 90 to 50% upon the temperature increase from 250 to 550 °C. As shown by our DFT calculations (Fig. 5), these experimental results cannot be explained based on the equilibrium segregation of the planar surface, for which only a maximum of 50% Au can be obtained.

Segregation is a phenomenon that depends on a complex interplay of both thermodynamic driving forces (including relative surface energies of alloy components, atomic-size mismatch, and pairwise interactions of heteroatoms) and the kinetic obstacles such as diffusion barriers. Because of the important role of the kinetic obstacles in a segregation process, elevated temperature is often needed to enhance the atom mobility and reach equilibrium. However, the increase in the crystal temperature also dramatically increases the concentration of thermal vacancies in the bulk. The equilibrium vacancy concentration is given by $N_v = \exp(\frac{\Delta S}{R})\exp(\frac{-\Delta H}{RT})$, where ΔS is the configuration entropy due to the vacancy-induced randomness in the bulk of the alloy system (the surface contribution to the entropy changes is considered negligible because of the small fraction of surface atoms compared with the bulk), and ΔH is the vacancy formation enthalpy. As obtained from our DFT calculations, the vacancy formation energies are 0.75 and 1.53 eV, respectively, for Cu and Au vacancies in the Cu_3Au bulk. Figure 7 shows the equilibrium concentrations of Cu and Au vacancies in the bulk as the temperature increases from 250 to 500 °C in our experiment. The vacancy concentrations are practically zero at 250 °C and increase rapidly with temperature. Particularly, the concentration of Cu vacancies is much higher than that for Au vacancies. For instance, the Cu vacancy concentration is five orders of magnitude larger than the Au vacancy concentration at 500 °C.

The observed temperature-dependent surface composition evolution of the Cu_3Au crystal can be well explained by
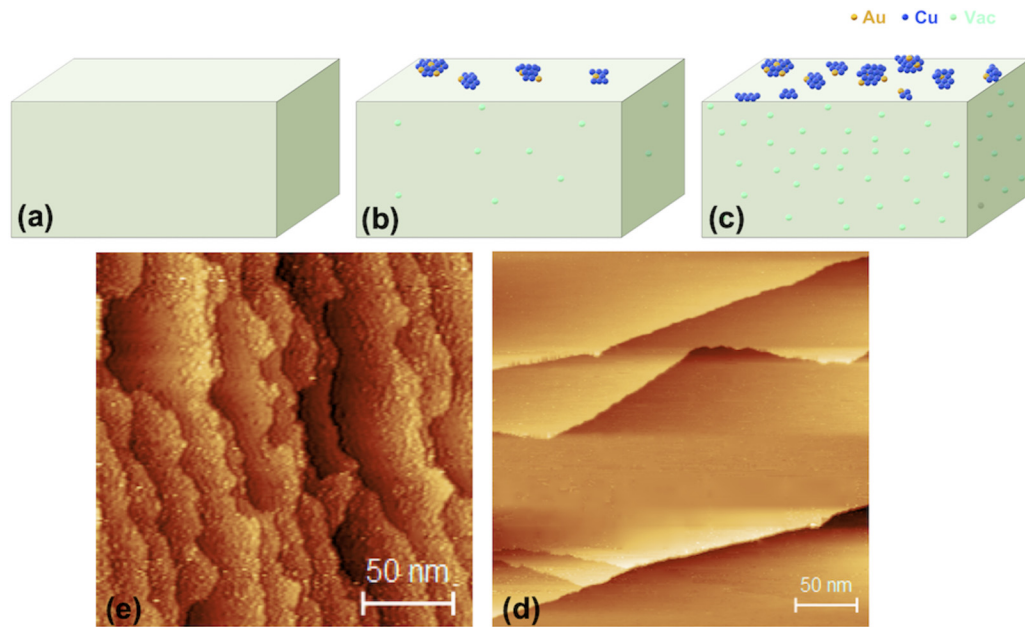
FIG. 8. (a)–(c) Schematic illustrations showing that the heating increases the concentration of bulk thermal vacancies, resulting in atoms being transferred from the bulk to the surface as adatoms that subsequently aggregate into clusters on the original surface. These clusters of adatoms become increasingly Cu rich as the temperature increases because of the lower vacancy formation energy and diffusion barriers for Cu atoms than those of Au atoms. (d) Scanning tunneling microscopy (STM) image of the $Cu_3Au(100)$ quenched rapidly from 500 °C to room temperature. (e) STM image of the $Cu_3Au(100)$ that was slowly cooled from 500 °C to room temperature.

the temperature-change-induced creation (or annihilation) of thermal vacancies in the bulk. Initially, a planar surface is presumed [Fig. 8(a)]. Upon the increase in temperature, the concentration of bulk thermal vacancies increases significantly, which in turn results in many mobile atoms that are expelled from the bulk and form as adatoms on the originally flat surface. These adatoms are Cu rich because of the lower vacancy formation energy for Cu (0.75 eV per Cu vacancy) than Au (1.53 eV per Au vacancy). The supply of Cu atoms from the bulk to the surface is also kinetically more favorable than that of Au atoms. As shown in our NEB calculations, the migration energy barriers for a Cu atom diffusing to an adjacent Cu vacancy and Au vacancy in the bulk are 0.65 and 0.43 eV, respectively, both of which are much lower than that (1.01 eV) for the diffusion of an Au atom to an adjacent vacant site. These adatoms subsequently aggregate into Cu-rich clusters (islands) on the surface [Fig. 8(b)]. Therefore, the original first layer atoms in the regions covered by the newly formed clusters now become the subsurface layer of the clusters [Fig. 8(c)]. As a result, the Au signals in XPS and LEIS from the original first layer atoms are attenuated by the clusters of adatoms. By contrast, the Cu signal, as detected by LEIS, becomes stronger because of the presence of the Cu-rich clusters. The further increase in temperature results in the transfer of more atoms from the bulk onto the surface, thereby developing a larger surface coverage of the Cu-rich clusters [Fig. 8(c)] and thus leading to the additional decrease in the Au signals detected by XPS and LEIS shown in Figs. 2–5. The temperature-driven clustering of adatoms is also confirmed experimentally by STM imaging of the surface morphology evolution. Figure 8(d) is an STM image showing the surface morphology of the $Cu_3Au(100)$ that is first annealed at 500 °C and then quenched to room temperature for STM imaging.

The observed appearance of a high density of particles at the surface is related to the quenched clusters of adatoms due to the rapid cooling.

Thermodynamically, the thermally driven adatoms tend to migrate back into the bulk as the temperature decreases. Kinetically, however, this process may not be fully reversible because of the energy barriers required for the inward migration of Au and Cu adatoms into the bulk. This is particularly the case for Au adatoms because the larger atomic size of Au makes it more difficult than Cu to migrate into the bulk at the lower temperature. Therefore, the adatoms evolve from being Cu rich to Au rich as the temperature decreases (Figs. 3 and 4) because of the incorporation of more Cu adatoms into the bulk. Equilibrium segregation may be achieved after prolonged annealing, by which adatoms can be fully incorporated into the bulk and/or surface steps, and the surface thus evolves into the planar morphology with the bulk termination. This is confirmed by our STM imaging of the $Cu_3Au(100)$ crystal that was slowly cooled down to room temperature. As shown in Fig. 8(e), the surface of the well-annealed crystal consists of flat terraces and atomic steps within a large field of view, where the disappearance of surface clusters is because of the transfer of surface adatoms to the bulk, thereby reducing the bulk vacancy concentration at the low temperature. The resultant bulk surface termination was also confirmed by the LEED showing the presence of superlattice diffraction spots [Fig. 1(b)].

Surfaces are the sources (or sinks) for the formation (or annihilation) of thermal vacancies in the bulk. For instance, it has been shown that oscillating the temperature of a NiAl(110) crystal instantly leads to the oscillating motions of atomic steps at the surface by accretion or reduction of thermal vacancies in the bulk [60,61]. That is, with increasing

temperature, bulk atoms migrate to the surface and form as adatoms because the concentration of thermal vacancies in the bulk increases; decreasing temperature makes the adatoms return to the bulk, thereby reducing the bulk vacancy concentration and restoring equilibrium in the bulk. The increased concentration of bulk thermal vacancies at the higher temperature results in the formation of more clusters at the surface. Therefore, a change in temperature can result in a net mass flux out of the bulk or into the bulk that equilibrates the crystal through vacancy creation or annihilation at the surface. This coupling between the bulk and surface is both intrinsic and inescapable and should have the consequence on the temperature-driven surface segregation phenomena. In fact, early experimental work analyzing the surface composition of the $Cu_3Au(100)$ suggested the existence of vacancies and adatoms at elevated temperatures [16,23]. Consistently, we observe that the mass transfer to/from the surface with temperature changes makes pronounced contributions to the dynamic evolution of both the surface composition and morphology. The observations point to the important role of the temperature-change-driven mass exchanges between the surface and bulk in influencing surface properties. Particularly, the formation of Cu-rich clusters, as revealed from the XPS and LEIS measurements, relies on the inherent differences in the vacancy formation energies of Cu and Au atoms in the Cu_3Au alloy, where the lower vacancy formation energy of Cu results in the enrichment of Cu adatoms at the surface. The observations made here for the stoichiometric $Cu_3Au(100)$ crystal also show clear differences from a $Cu_{90}Au_{10}$ solid solution. The latter has a lower surface stability (due to the less abundant pairwise Cu-Au atomic interactions in the Cu-rich solid solution) during the high-temperature annealing of the thin film sample, for which the step-edge detachments at active surface sites (e.g., atomic steps, kinks, ledges) results in many Cu and Au adatoms, and the disparity in the adatom-substrate exchange barriers results in the significant enrichment of solute atoms that subsequently aggregate as Au-rich clusters or an Au-rich surface layer [62,63].

We envision the broader applicability of the identified coupling between the surface segregation dynamics and temperature-change-driven surface-bulk mass exchanges. This is because the disparity in the vacancy formation energies of dissimilar atoms in multicomponent materials naturally leads to the different concentrations of the bulk thermal vacancies of the dissimilar atoms. The transfer of the excess atoms from/to the bulk with the temperature changes results in the disparity in the surface enrichment or depletion of the constituent atoms. Other extended defects, such as dislocation cores, stacking faults, grain boundaries in polycrystal materials, and phase boundaries in heterogeneous materials can also serve as sources (or sinks) of thermal vacancies in the bulk. It can be reasonably expected that the disparity in the equilibrium concentrations of thermal vacancies of the constituent

atoms in multicomponent materials can also result in the composition inhomogeneities at these internal defects through the temperature-change-driven mass exchanges between the extended defects and the surrounding bulk area because of the creation and annihilation of thermal vacancies.

V. CONCLUSIONS

We have identified an adatom mechanism underlying the transient surface segregation phenomena of $Cu_3Au(100)$ under nonisothermal conditions. It is shown that the surface Au decreases monotonically with the temperature increasing from 250 to 500 °C. Based on our experimental measurements and atomistic modeling, we conclude that the temperature-change-driven mass exchanges between the surface and bulk are responsible for the evolution of the surface composition and morphology. That is, the lower vacancy formation energy for Cu than Au in Cu_3Au results in more bulk thermal vacancies of Cu with the increase in temperature, for which the excess Cu atoms are expelled onto the surface as adatoms that aggregate as Cu-rich clusters. Decreasing temperature drives more Cu adatoms than Au adatoms back to the bulk, thereby making the adatoms Au rich. This surface-bulk mass flow allows the surface to change its composition by the partitioning of the alloying elements to the free surface. We expect the broader applicability of this finding because of the inherent differences in the vacancy formation energies of dissimilar atoms in multicomponent materials and the generality of free surfaces (and internal interfaces) as the sources (or sinks) of bulk thermal defects in modulating the surface composition via the disparity in surface-bulk exchanges of the constituent atoms.

[1] J. A. Rodriguez, Physical and chemical properties of bimetallic surfaces, Surf. Sci. Rep. **24**, 223 (1996).

[2] M. Polak and L. Rubinovich, The interplay of surface segregation and atomic order in alloys, Surf. Sci. Rep. **38**, 127 (2000).

[3] P. A. Dowben and A. Miller, *Surface Segregation Phenomena* (CRC Press, Boca Raton, 1990).

[4] L. F. Zou, W. A. Saidi, Y. K. Lei, Z. Liu, J. Li, L. Li, Q. Zhu, D. Zakharov, E. A. Stach, J. C. Yang, G. F. Wang, and

G. W. Zhou, Segregation induced order-disorder transition in Cu(Au) surface alloys, Acta Mater. **154**, 220 (2018).

[5] B. Han, A. Van der Ven, G. Ceder, and B.-J. Hwang, Surface segregation and ordering of alloy surfaces in the presence of adsorbates, Phys. Rev. B **72**, 205409 (2005).

[6] B. A. Front, B. Legrand, G. Tréglia, and C. Mottet, Bidimensional phases in Co-Pt surface alloys: A theoretical study of ordering and surface segregation, Surf. Sci. **679**, 128 (2019).

[7] W. Chen, P. Dalach, F. Schneider, and C. Wolverton, Interplay between subsurface ordering, surface segregation, and adsorption on Pt-Ti(111) near-surface alloys, Langmuir **28**, 4683 (2012).

[8] A. Lopes, G. Treglia, C. Mottet, and B. Legrand, Ordering and surface segregation in CoPt nanoparticles: A theoretical study from surface alloys to nanoalloys, Phys. Rev. B **91**, 035407 (2015).

[9] A. Hizia, A. Front, M. Said, F. Berthierc, G. Tréglia, and C. Mottet, Tight-binding Ising modeling of the interplay between bulk ordering and surface segregation in Pt-Ag nanoalloys, Surf. Sci. **700**, 121626 (2020).

[10] Y. Zhang, G. Kresse, and C. Wolverton, Nonlocal First-Principles Calculations in Cu-Au and Other Intermetallic Alloys, Phys. Rev. Lett. **112**, 075502 (2014).

[11] L. F. Zou, J. Li, D. Zakharov, W. A. Saidi, E. A. Stach, and G. W. Zhou, Atomically visualizing elemental segregation induced surface alloying and restructuring, J. Phys. Chem. Lett **8**, 6035 (2017).

[12] L. F. Zou, C. M. Yang, Y. K. Lei, D. Zakharov, J. M. K. Wiezorek, D. Su, Q. Y. Yin, J. Li, Z. Y. Liu, E. A. Stach, J. C. Yang, L. Qi, G. F. Wang, and G. W. Zhou, Dislocation nucleation facilitated through atomic segregation, Nat. Mater. **17**, 56 (2018).

[13] M. A. Vasiliev, Surface effects of ordering in binary alloys, J. Phys. D: Appl. Phys. **30**, 3037 (1997).

[14] M. Polak and L. Rubinovich, Alloy surface segregation and ordering phenomena: recent progress, in *The Chemical Physics of Solid Surfaces* (Elsevier, Amsterdam, 2002), Vol. 10, pp. 86–117.

[15] H. M. Polatoglou and P. Cafarelli, Effect of the [001] surface of Cu₃Au on the order-disorder transition, Surf. Sci. **352-354**, 972 (1996).

[16] H. Reichert, P. J. Eng, H. Dosch, and I. K. Robinson, Thermodynamics of Surface Segregation Profiles at Cu₃Au(001) Resolved by X-Ray Scattering, Phys. Rev. Lett. **74**, 2006 (1995).

[17] L. G. Dias, A. A. Leitao, C. A. Achete, R.-P. Blum, H. Niehus, and R. B. Capaz, Chemical identification in the Cu₃Au(100) surface using scanning tunneling microscopy and first-principles calculations, Surf. Sci. **601**, 5540 (2007).

[18] H. Niehus and C. Achete, Surface-structure investigation of nitrogen and oxygen on Cu₃Au(100), Surf. Sci. **289**, 19 (1993).

[19] L. Houssiau and P. Bertrand, Observation of surface rippling on Cu₃Au(100) with ToF-ISS, Nucl. Instr. Meth. B **115**, 161 (1996).

[20] T. M. Buck, G. H. Wheatley, and L. Marchut, Order-Disorder and Segregation Behavior at the Cu₃Au(001) Surface, Phys. Rev. Lett. **51**, 43 (1983).

[21] E. G. McRae, T. M. Buck, R. A. Malic, W. E. Wallace, and J. M. Sanchez, Ordering and layer composition at the Cu₃Au(110) surface, Surf. Sci. **238**, L481 (1990).

[22] L. Houssiau and P. Bertrand, Order-disorder phase transition of the Cu₃Au(100) surface studied by ToF-Ion scattering, Nucl. Instr. Meth. B **118**, 467 (1996).

[23] D. H. Oh, H. J. Kang, K. H. Chae, C. N. Whang, B. V. King, D. J. O'Connor, and D. W. Moon, Compositional changes in the surface layers of the Cu₃Au(1 0 0) below the bulk transition temperature, Surf. Sci. **477**, L289 (2001).

[24] H. Reichert and H. Dosch, Surface segregation in Cu₃Au(001), Surf. Sci. **345**, 27 (1996).

[25] H. Dosch and H. Reichert, Ordering, disordering and segregation at binary interfaces: model system Cu₃Au(001), Acta Mater. **48**, 4387 (2000).

[26] I. Zasada, L. Rok, S. Mroz, and T. Rychtelska, Nucleation process in Cu₃Au(001) surface region around the order-disorder phase transition, J. Chem. Phys. **133**, 234706 (2010).

[27] I. Zasada, L. Wojtczak, and S. Mróz, Layer dependent composition of AuCu₃(100) in the semi-infinite and thin film geometry, J. Alloys Comp. **469**, 593 (2009).

[28] A. Van der Ven, H. C. Yu, G. Ceder, and K. Thornton, Vacancy mediated substitutional diffusion in binary crystalline solids, Prog. Mater. Sci. **55**, 61 (2010).

[29] N. H. Protik, J. Carrete, N. A. Katcho, N. Mingo, and D. Broido, *Ab initio* study of the effect of vacancies on the thermal conductivity of boron arsenide, Phys. Rev. B **94**, 045207 (2016).

[30] Y. Kraftmakher, Equilibrium vacancies and thermophysical properties of metals, Phys. Rep. **299**, 79 (1998).

[31] Y. Lee, S. Lee, and G. S. Hwang, Effects of vacancy defects on thermal conductivity in crystalline silicon: A nonequilibrium molecular dynamics study, Phys. Rev. B **83**, 125202 (2011).

[32] J. J. Olivero and R. L. Longbothum, Empirical fits to the Voigt line width: a brief review, J. Quant. Spectrosc. Radiat. Transfer **17**, 233 (1977).

[33] D. A. Shirley, High-resolution x-ray photoemission spectrum of the valence bands of gold, Phys. Rev. B **5**, 4709 (1972).

[34] G. Kresse and J. Furthmuller, Efficient iterative schemes for *ab initio* total-energy calculations using a plane-wave basis set, Phys. Rev. B **54**, 11169 (1996).

[35] G. Kresse and D. Joubert, From ultrasoft pseudopotentials to the projector augmented-wave method, Phys. Rev. B **59**, 1758 (1999).

[36] J. P. Perdew, K. Burke, and M. Ernzerhof, Generalized Gradient Approximation Made Simple, Phys. Rev. Lett. **77**, 3865 (1996).

[37] H. J. Monkhorst and J. D. Pack, On special points for Brillouin-zone integrations, Phys. Rev. B **13**, 5188 (1976).

[38] E. G. McRae and R. A. Malic, Observations of the Cu₃Au(001) phase transition using a novel low energy electron diffraction system, Surf. Sci. **148**, 551 (1984).

[39] J. M. Sanchez and J. L. Morán-López, Ordering and segregation at (001) surfaces of Cu₃Au, Surf. Sci. Lett. **157**, L297 (1985).

[40] F. M. Zhang, B. V. King, and D. J. O'Connor, Low Energy Ion Scattering Investigation of the Order-Disorder Transition in the First Atomic Layer of the Cu₃Au(100) Surface, Phys. Rev. Lett. **75**, 4646 (1995).

[41] J. Greeley and M. Mavrikakis, Surface and subsurface hydrogen: adsorption properties on transition metals and near-surface alloys, J. Phys. Chem. B **109**, 3460 (2005).

[42] B. Hammer and J. K. Norskov, Why gold is the noblest of all the metals, Nature **376**, 238 (1995).

[43] C. R. Li, Q. Q. Liu, J. A. Boscoboinik, and G. W. Zhou, Tuning the surface composition of Cu₃Au binary alloy, Phys. Chem. Chem. Phys. **22**, 3379 (2020).

[44] M. Pan, A. J. Brush, Z. D. Pozun, H. C. Ham, W.-Y. Yu, G. Henkelman, G. S. Hwang, and C. B. Mullins, Model studies of heterogeneous catalytic hydrogenation reactions with gold, Chem. Soc. Rev. **42**, 5002 (2013).

[45] K. Mudiyanselage, Y. Yang, F. M. Hoffmann, O. J. Furlong, J. Hrbek, M. G. White, P. Liu, and D. J. Stacchiola, Adsorption of hydrogen on the surface and sub-surface of Cu(111), J. Chem. Phys. **139**, 044712 (2013).

[46] M. Okada, Y. Tsuda, K. Oka, K. Kojima, W. A. Diño, A. Yoshigoe, and H. Kasai, Experimental and theoretical studies on oxidation of Cu-Au alloy surfaces: effect of bulk Au concentration, Sci. Rep. **6**, 31101 (2016).

[47] Y. Tsuda, K. Oka, T. Makino, M. Okada, W. A. Diño, M. Hashinokuchi, A. Yoshigoe, Y. Teraoka, and H. Kasai, Initial stages of Cu₃Au(111) oxidation: oxygen induced Cu segregation and the protective Au layer profile, Phys. Chem. Chem. Phys. **16**, 3815 (2014).

[48] K. Oka, Y. Tsuda, T. Makino, M. Okada, M. Hashinokuchi, A. Yoshigoe, Y. Teraoka, and H. Kasai, The effects of alloying and segregation for the reactivity and diffusion of oxygen on Cu₃Au(111), Phys. Chem. Chem. Phys. **16**, 19702 (2014).

[49] S. B. DiCenzo, P. H. Citrin, E. H. Hartford, and G. K. Wertheim, Au surface density of states and surface core-level shifts in Cu₃Au(001), Phys. Rev. B **34**, 1343 (1986).

[50] M. Okada, M. Hashinokuchi, M. Fukuoka, and T. Kasai, Protective layer formation during oxidation of Cu₃Au(100) using hyperthermal O₂ molecular beam, Appl. Phys. Lett. **89**, 201912 (2006).

[51] M. Okada, K. Moritani, T. Fukuyama, H. Mizutani, A. Yoshigoe, Y. Teraoka, and T. Kasai, Comparative study of oxidation on Cu and Cu₃Au surfaces with a hyperthermal O₂ molecular beam, Surf. Sci. **600**, 4228 (2006).

[52] W. Eberhardt, S. C. Wu, R. Garrett, D. Sondericker, and F. Jona, Core-level shifts and the electronic structure of Cu₃Au, Phys. Rev. B **31**, 8285 (1985).

[53] M. Kuhn and T. K. Sham, Charge redistribution and electronic behavior in a series of Au-Cu alloys, Phys. Rev. B **49**, 1647 (1994).

[54] R. G. Jordan, Y. Jiang, M. A. Hoyland, and A. M. Begley, Investigation of the electronic structure in Cu-Au I using x-ray-photoelectron spectroscopy, Phys. Rev. B **43**, 12173 (1991).

[55] M. D. Moreira, First-principles calculations and XPS measurements of gold segregation at the Cu₃Au(111) Surface, J. Vac. Sci. Tech. B **30**, 051802 (2012).

[56] C. Mannori, T. Scimia, P. Cantini, S. Terreni, M. Canepa, and L. Mattera, The Cu₃Au (001) surface: a He diffraction study, Surf. Sci. **433-435**, 307 (1999).

[57] S. Pandey, R. J. Koch, G. Li, S. T. Misture, H. Wang, and S. R. Phillpot, Thermodynamics and kinetics of ordered and disordered Cu/Au alloys from first principles calculations, J. Alloys Comp. **809**, 151615 (2019).

[58] F. Chiter, V. B. Nguyen, N. Tarrat, M. Benoit, H. Tang, and C. Lacaze-Dufaure, Effect of van der Waals corrections on DFT-computed metallic surface properties, Mater. Res. Express **3**, 046501 (2016).

[59] G. Henkelman, B. P. Uberuaga, and H. Jónsson, A climbing image nudged elastic band method for finding saddle points and minimum energy paths, J. Chem. Phys. **113**, 9901 (2000).

[60] K. F. McCarty, J. A. Nobel, and N. C. Bartelt, Vacancies in solids and the stability of surface morphology, Nature **412**, 622 (2001).

[61] K. F. McCarty, J. A. Nobel, and N. C. Bartelt, Surface dynamics dominated by bulk defects: the case of NiAl(110), Phys. Rev. B **71**, 085421 (2005).

[62] L. F. Zou, P. Cao, Y. Lei, D. Zakharov, X. Sun, S. House, L. Luo, J. Li, Y. Yang, Q. Yin, X. Chen, C. Li, H. Qin, E. A. Stach, J. C. Yang, G. Wang, and G. W. Zhou, Atomic-scale phase separation induced clustering of solute atoms, Nat. Commun. **11**, 3934 (2020).

[63] K. Liu, S. M. Zhang, D. X. Wu, L. L. Luo, X. H. Sun, X. B. Chen, D. Zakharov, S. Cheng, Y. Zhu, J. C. Yang, G. F. Wang, and G. W. Zhou, Effect of surface steps on chemical ordering in the subsurface of Cu(Au) solid solutions, Phys. Rev. B **103**, 035401 (2021).